Influence of polypropylene and steel fibres on thermal spalling and physical-mechanical properties of concrete under different heating rates

N. Algourdin, P. Pliya, A.-L. Beaucour, A. Simon, A. Noumowé

Influence of polypropylene and steel fibres on thermal spalling and physical-mechanical properties of concrete under different heating rates

N. Algourdin[2], P. Pliya[1], A.-L. Beaucour[1*], A. Simon[3], A. Noumowé[1]

[1] *CY Cergy Paris Université, Laboratory of Mechanics and Materials of Civil Engineering (L2MGC), EA 4114, F-95000 Cergy-Pontoise, France*

[2] *Université de Lyon, Laboratoire de Tribologie et Dynamique des Systèmes (LTDS), UMR 5513, 58 rue Jean Parot, 42023 Ecole Nationale d'Ingénieurs de Saint-Etienne, France*

[3]*EIFFAGE Génie-Civil, 3-7 place de l'Europe, 78140 Vélizy Villacoublay, France*

[*]*Corresponding author:*

email: anne-lise.beaucour@cyu.fr

phone: +33 (0)1 34 25 69 75

Abstract

This study investigates three concrete compositions: a control concrete, a reinforced concrete containing 60 kg/m^3 of steel fibres, and a hybrid concrete containing 60 kg/m^3 of steel fibres and 0.75 kg/m^3 of polypropylene fibres. Cylindrical specimens were manufactured and subjected to two heating rates (10 °C/min and the ISO 834 fire standard) to study their spalling sensitivity. Moreover, unidirectional heat transfer and pressure measurements were performed on slabs heated at 10 °C/min to 600 °C. To understand the influence of fibres on spalling processes more clearly, the thermal properties were studied during heating and cooling: the gas permeability, compressive strength, and Young's modulus of specimens were measured after a heating and cooling cycle at 0.5 °C/min. The results show that the spalling phenomenon was more severe for cylindrical specimens than for slabs. The addition of 60 kg/m^3 of steel fibres had an unfavourable influence on spalling, especially during the ISO 834 fire test. The addition of 0.75 kg/m^3 of polypropylene fibres allowed the concretes containing steel fibres to avoid spalling, regardless of the thermal loading conditions.

Keywords

Polypropylene fibres, steel fibres, high-strength concrete, pore pressure, high temperatures, heating rate, spalling, gas permeability, thermal conductivity, specimen geometry.

Introduction

Fire safety is one of the key aspects in the design of structures. Concrete preparation methods have changed significantly in recent decades. Since the 1990's, high-strength concretes have become increasingly common. However, high-strength concretes exposed to high temperatures exhibit a tendency to undergo explosive spalling, thus leading to direct fire exposure of the steel rebar and a reduction in the cross-sectional area. Despite significant advances in research, thermal spalling remains a complex problem. Two physical mechanisms are often associated with this phenomenon: (a) thermal dilatation/shrinkage gradients and (b) the build-up of pore pressure [1–4]. On one hand, the thermal gradient generated across a concrete member section results in restrained thermal expansion, which leads to a build-up of compressive stress near the concrete surface and tensile stress in the concrete interior. Biaxial compressive thermal stresses parallel to the heated surface can lead to concrete spalling [5,6]. The second mechanism is related to the water pressure increase within the concrete during heating. The pressure and concentration gradient drive vapour not only out of the concrete element, but also to the colder part of the concrete, where the water vapour condenses due to the temperature change. The accumulation of liquid water leads to local saturation of the pores [7–9]. This "moisture clog" reduces the movement of water vapour, leading to an increase in the gas pore pressure. The generation of this high pore pressure contributes to explosive spalling of the concrete [6,10,11]. An important thermo-hydrous point is the expansion and vaporisation of water within a few minutes after the temperature has reached its critical point inside the concrete structure. The pore pressure acts as a trigger for spalling. When the cracking process starts, a rapid pressure release occurs. Nevertheless, the spalling mechanisms progress due to the already generated strong localisation of damage and increasing thermo-mechanical stresses [12].

Liu et al. [13] have suggested a new perspective for fire-induced concrete spalling depending on thermo-chemical spalling, which is related to the decomposition of hydrated products and calcite and the rehydration of calcium oxide. All of these mechanisms are simultaneous and involve complex coupled thermo–hydro–mechanical (THM) processes [14,15]. The occurrence of spalling depends on the rate at which the pore pressure and thermal stresses increase and the material strength decreases [4,16]. These mechanisms are related to intrinsic parameters of the material such as transfer (mass and heat) and mechanical properties; they are also related to environmental conditions such as the geometry of the element, moisture conditions, boundary conditions, and the heating rate [17]. In one scenario, the concrete may

not spall at all, whereas in another scenario, with different geometry or thermal loading, it may spall severely. Indeed, the contribution of each of the mechanisms as the cause of the spalling can vary according to these conditions. The various aspects of spalling (surface spalling, explosive spalling, corner spalling, and aggregate spalling) that can be observed illustrate the complexity of the THM coupling and the plurality of the involved mechanisms [18]. This is the reason that there is not a consensus agreement on the relative contribution of the influencing factors to the spalling phenomenon. The factors contributing to spalling are often considered to be low concrete permeability, large thermal and hygric gradients, and fast moisture migration [4]. A high heating rate can be considered an unfavourable factor, as it can generate high thermal and hygric gradients. However, according to some other authors, higher heating rates lead to lower pore pressures due to the occurrence of surface cracking [6]. A large amount of water vapour can escape to the outside of the specimen and cracking can create more space for vapour and liquid water to expand, thus decreasing the internal pressure and spalling of the concrete [10,19]. Gawin et al. [20] compared the heat and mass transfer under two heating rates (ISO 834 fire standard and 2 °C/min) through a numerical study. Lower values of the temperature gradient, moisture content, and pressure were observed under the lower heating rate, resulting in approximately 2–3 times smaller mass flows and approximately 10–20 times smaller heat flows at a given temperature. For slow heating (2 °C/min), the maximum values of the liquid moisture saturation and gas and vapour pressure were slightly higher and occurred at distances 2–4 times further from the surface compared to those observed during fast heating (ISO 834 fire standard).

The boundary conditions also have an effect on the degree of spalling. On one hand, asymmetric heating amplifies thermal stresses and moisture gradients [21]. The worst results were obtained with a “one-side heating condition” and a specimen with a large surface (slab), because this type of specimen stores more energy for a given heating condition [22]. On the other hand, the one-side heating condition allows vapour to migrate out from the unexposed parts of the specimen. Some studies have shown that water can escape through cracks on the unexposed surfaces, thus decreasing the risk of spalling [23]. The degree of spalling is also affected by the structural size. Indeed, the larger the column diameter, the greater the thermal gradient will be [22]. However, Conolly [24] concluded that thicker concrete specimens are less likely to experience explosive spalling. Jansson et al. [25] compared spalling results for large and small slabs with the same thickness and type of loading system. Small slabs of 600

× 500 × 200 mm^3 spalled substantially less compared with large slabs of 1800 × 1200 × 200 mm^3.

To prevent concrete fire spalling, polypropylene fibres can be added [26–29]. Polypropylene fibres start to expand and then melt at 160–170 °C and are absorbed by the porous network of the cement matrix [1]. The void spaces left by these fibres can be considered as weak points inside the concrete and the thermal stresses will cause additional cracks at the edges of the voids [30,31]. This allows for the formation of an interconnected network [5]. Fibres decrease the pore pressure because of the increased concrete permeability [10]. Steel fibres have an effective role in limiting the loss of mechanical performance with temperature. With regard to spalling, the action of steel fibres has not been definitively established. Some experimental studies have shown that adding steel fibres is beneficial for reducing spalling [32–34]. Bangi et al. [35] highlighted the contribution of steel fibres in reducing the pore pressure in deeper regions of the concrete during rapid heating. Other authors have reported that explosive spalling occurs when steel fibres are added to the concrete mix [36,37]. This could be due to the capacity of steel fibres to reduce crack opening and limit water evacuation [5]. According to Varona et al. [38], the high aspect ratio of steel fibres may make them more prone to lose bond to the concrete matrix because of oxidation at high temperatures.

It is important to achieve a better understanding of the action of steel fibres and hybrid fibres on concrete spalling behaviour. Considering the contradictory reported findings and the influence of environmental conditions, the effectiveness of steel fibres should be investigated under different heating rates, boundary thermal conditions, and specimen geometries. The aim of this study, by varying the heating conditions, is to achieve a better understanding of the mechanisms involved in spalling phenomena and how steel and hybrid fibres modify the behaviour of high-strength concrete at high temperatures. This study investigates three concrete mixtures: a reference concrete (Cref), a reinforced concrete containing 60 kg/m^3 of steel fibres (CS 60), and a hybrid concrete containing 60 kg/m^3 of steel fibres and 0.75 kg/m^3 of polypropylene fibres (CS 0.75-60). Tests were conducted with two heating rates (ISO 834 fire standard and 10 °C/min). One-side heating with slab specimens and all-side heating with cylindrical specimens were performed. To understand the influence of fibres on spalling processes, the evolution of the physical and mechanical properties of the concretes with temperature was investigated. Thermal properties (thermal conductivity, specific heat) were also studied during heating and cooling. After different heating–cooling temperatures, the gas permeability, compressive strength, and modulus of elasticity were measured. For this part of

the study, the heating and cooling rate was maintained at 0.5 °C/min to ensure homogeneity of the temperature and limit thermal gradients in the specimens.

1. Experimental schedule

1.1 Concrete constituents

Cement: The cement used was CEM I 52.5 N from Villiers-au-Bouin (Table 1). The cement density was 3.13 kg/dm^3, and the compressive strength measured in standard mortar at 28 (d) was 61.3 MPa with a water/cement ratio (W/C) of 0.5 [39].

Table 1 Chemical and physical composition of the CEM I 52.5 N cement

Composition [%]	
Clinker	97
Gypsum	3
Chemical composition [%]	
CaO	62.0
SiO_2	20.1
Al_2O_3	4.6
SO_3	3.1
Fe_2O_3	2.4
MgO	2.0
Physical properties	
Density [kg/m^3]	3100
Blaine surface [cm^2/g]	4400

Aggregates: A limestone aggregate of Tournaisis composed of calcareous (87–91%) and quartz (9–13%) was used in this study. The sand and gravel were supplied as 4/10 and 10/20 aggregate classes, respectively. The specific gravity of both aggregates was 2.67 kg/m^3.

Superplasticiser: Cimfluid 2002 polycarboxylate-based superplasticiser was used. The superplasticiser density was 1.1 kg/dm^3, and the dry extract was 35%.

Fibres: Monofilament cylindrical polypropylene fibres (PPF) of Duomix M12 (BEKAERT) and high-carbon galvanised steel fibres (SF) of Dramix RC-80/30-CP (BEKAERT) with hooked ends were used. Table 2 specifies the properties of the PPF and SF.

Table 2 Fibre properties

	Fibre	*Diameter*	*Length (mm)*	*Density (g/cm^3)*	*Tensile strength (N/mm^2)*	*Modulus of elasticity (N/mm^2)*
PPF	Duomix M12	32 µm	12	0.91	250 ±15%	3500–3900
SF	Dramix RC-80/30-CP	0.38 mm	30	7.80	3070 ± 7.5%	210,000

1.2 Concrete mixtures

Three mixtures of high-strength concrete were investigated: concrete without fibres (Cref), concrete with 60 kg/m^3 of steel fibres (CS 60), and concrete with 0.75 kg/m^3 of polypropylene fibres and 60 kg/m^3 of steel fibres (CPPS 0.75-60).

All the mixes had the same W/C ratio of 0.38 with 475 kg/m^3 of cement. The slump of the concretes without fibres ranged from 160 to 210 mm, whereas that of the concretes with fibres ranged from 100 to 150 mm. The concrete mix proportions (kg/m^3) are given in Table 3. The target was a C55/67 concrete compressive strength class.

Table 3 Mix proportions of concretes

	Mixture proportions (kg/m^3)							
Concretes	*Cement*	*Efficient water*	*Sand 0/4*	*Gravel 4/10*	*Superplasticiser (dry extract)*	*SF*	*PPF*	$f_{c\ 28\ days}$ *(MPa)*
Cref	475	181	885	884	1.0	-	-	65.2 ± 0.7
CS 60	475	181	867	866	2.85	60	-	79.0 ± 2.4
CPPS 0.75-60	475	181	867	865	2.99	60	0.75	81.3 ± 0.8

For each concrete mixture, 12 cylindrical specimens of ∅150 × 300 mm (diameter × height) were tested according to the ISO 834 fire standard. For the tests at 10 °C/min, two slabs of 600 × 300 × 120 mm per mixture (6 slabs in total) were also tested. To conduct the residual tests after slow heating (0.5 °C/min), 40 cylindrical specimens of ∅150 × 300 mm (diameter × height) were manufactured.

1.3 Specimen curing

Cylindrical specimens were kept in their moulds at 20 ± 2 °C for 7 d. Then, the specimens were removed from their moulds and stored in plastic bags with wet rags in order to avoid any water evaporation until the day of the test. The slabs were kept in plywood moulds with wet rags and covered with plastic bags until the test day. The specimens were cured for at least 90 d to ensure that the hydration reactions had stabilised and to reduce the interstitial water in the concrete.

1.4 Heating tests

1.4.1 ISO 834 fire test and spalling investigation

Type K thermocouples were placed in the furnace before heating and at the centre of the cylindrical concrete specimens during casting (Figure 1). Two specimens per mixture were equipped with thermocouples in the centre. Each thermocouple was connected to a data logger that recorded continuous measurements and transmitted them to the computer.

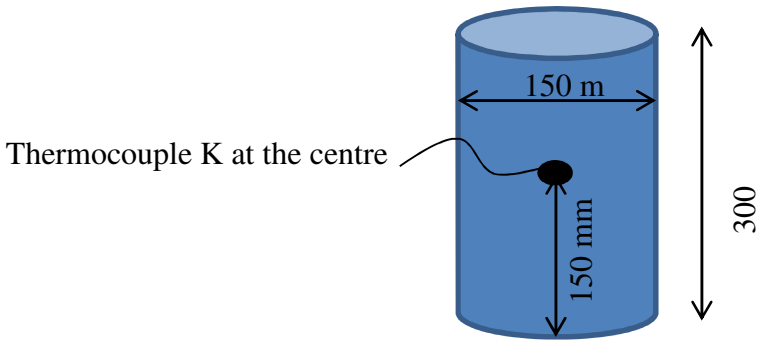

Figure 1 Position of the centre thermocouple inside a specimen

An ISO 834 fire test of two hours was performed on Ø150 × 300 mm cylindrical concrete specimens in a gas furnace (inner dimensions of 7000 × 5000 mm). The position of the specimens in the furnace and evolution of the maximum (T_{fmax}) and minimum (T_{fmin}) furnace temperatures compared to the ISO 834 fire standard curve are presented in Figure 2(a) and (b), respectively.

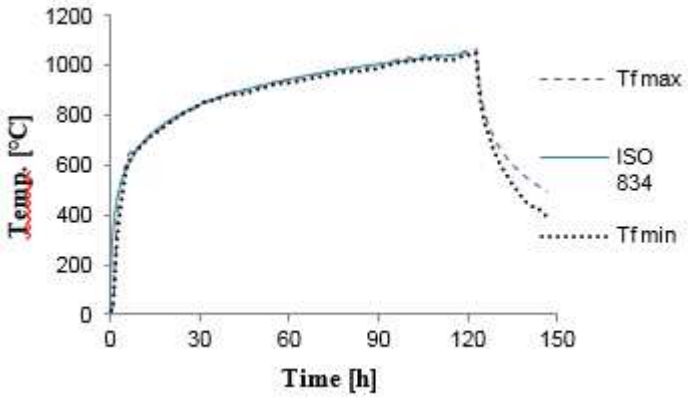

(a) (b)

Figure 2 (a) Specimens in the gas furnace and (b) evolution of the furnace temperatures compared to the standard ISO 834 fire curve

Spalling assessment methodology

After the ISO 834 fire test, spalling assessments were performed to provide a detailed analysis of the specimen degradation. Each specimen was weighed before and after the heating–cooling cycles. The maximum depth and percentage surface area loss due to spalling were measured. The spalled specimens were wrapped in tracing paper to draw the spalled surface. The spalled surfaces were then measured using AutoCad after scanning the images.

1.4.2 Heating test at 10 °C/min and spalling investigation

The temperature and pressure were measured within the slab during heating. Figure 3 shows the positions of the pressure and temperature gauges within the slab. Type K thermocouples were positioned on heated and not-heated faces and at different depths within the slabs.

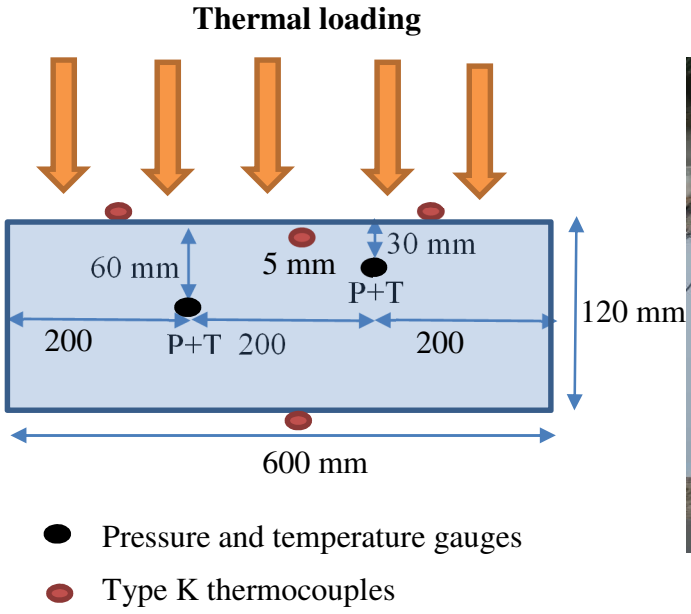

Figure 3 Scheme and photograph of the instrumentation within a slab

The 10 °C/min heating was performed in an electric furnace (Figure 4) (1300 × 1010 × 1040 mm) equipped with a ventilation system to homogenise the temperature inside the furnace. The connected data logger allowed for the temperature and pressure during heating to be recorded.

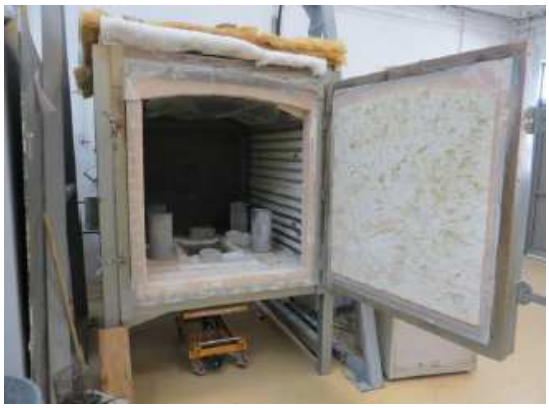

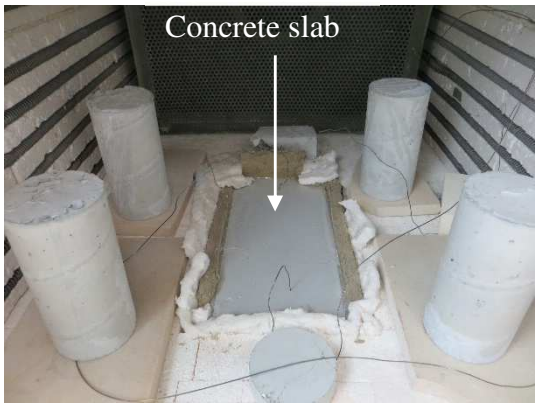

Figure 4 Outside and inside views of the electric furnace

Concrete slabs of 600 × 300 × 120 mm (length × width × thickness) and four cylindrical specimens of Ø150 × 300 mm were subjected to a heating rate of 10 °C/min from room temperature to 600 °C. The specimens were then rested for 4 h and subjected to controlled cooling from 600 °C to room temperature (Figure 5). As the essential chemical and physical reactions occur between 100 °C and 600 °C, the target heating temperature was limited to 600 °C. The 4-h rest time was chosen to obtain a temperature of 300 °C in the middle of the slab (60 mm). The slab specimen was situated on the bottom of the furnace. Its upper surface was exposed to high temperatures, whereas the other surfaces were thermally isolated using glass wool. The lateral sides were wrapped with self-adhesive aluminium foils. The resulting one-sided heating can be considered as a unidirectional heat and hydric flow.

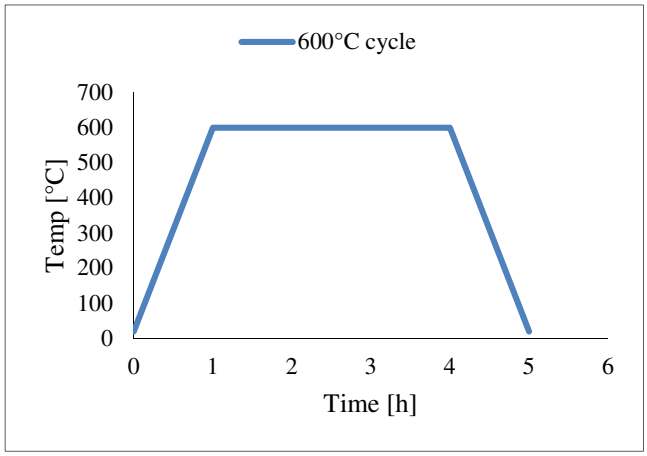

Figure 5 Thermal profile of the 10 °C/min heating–cooling cycle

Temperatures were measured on the heated and un-heated faces. A thermocouple located 5 mm below the exposed surface was embedded in the concrete before casting (T 5 mm). Figure 6 shows the temperature and pressure measuring device. Two stainless steel tubes were placed in the concrete before casting at 30 and 60 mm below the heated face to measure the pore pressure (P) and temperature (T 30 mm or 60 mm) simultaneously at the same point. The measurement instruments developed in this study were based on a an instrument previously developed by Kalifa et al. [11]. They included a cylindrical sintered metal tip (12.5 × 24.2 mm) fixed to a stainless steel tube (with an outer diameter of 3.2 mm and inner diameter of 1.6 mm). The tubes were empty. One end was used to connect a piezoelectric transducer. A thermocouple (diameter of 1 mm) was inserted into the other end of the tube until it touched

the cylindrical sintered metal tip. Thus, the vapour pressure and temperature could be measured simultaneously at the same position during heating of the concrete specimen. The presence of the thermocouple in the tube also reduced the dead volume. Another type K thermocouple was fixed in a small pore on the non-exposed surface ($T_{non\ exp.\ surf}$). The temperature of the furnace ($T_{furnace}$) was also measured using a type K thermocouple.

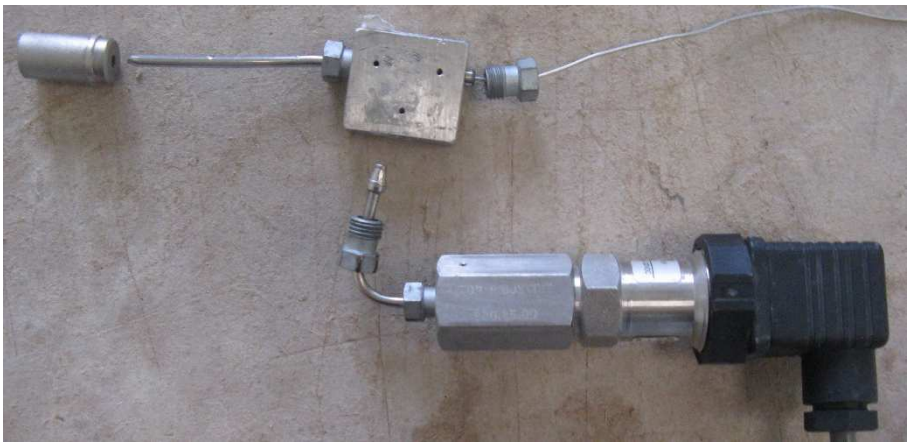

Figure 6 Temperature and pressure measurement device

Spalling assessment methodology

Modelling clay was used to estimate the volume of spalled concrete. The empty spaces generated by spalling were filled with the modelling clay. Then, the volume of the extracted modelling clay was determined by hydrostatic weighing. Furthermore, the spalling surface was estimated with the help of tracing paper in the same manner as after the ISO 834 fire tests.

1.4.3 Slow heating test at 0.5 °C/min and residual characterisation tests

The transfer and mechanical properties were studied using ∅150 × 300 mm concrete cylinders. The specimens were subjected to 300 °C, 450 °C, 600 °C, 750 °C, and 900 °C heating–cooling cycles (Figure 7). Each cycle included a phase of increasing temperature (0.5 °C/min), a temperature rest phase (one hour), and a cooling phase (0.5 °C/min). The heating rate of 0.5 °C/min was chosen according to the recommendations of RILEM 200-HTC [40]. To establish temperature-dependant material property laws, uniform temperatures had to be ensured within the specimen.

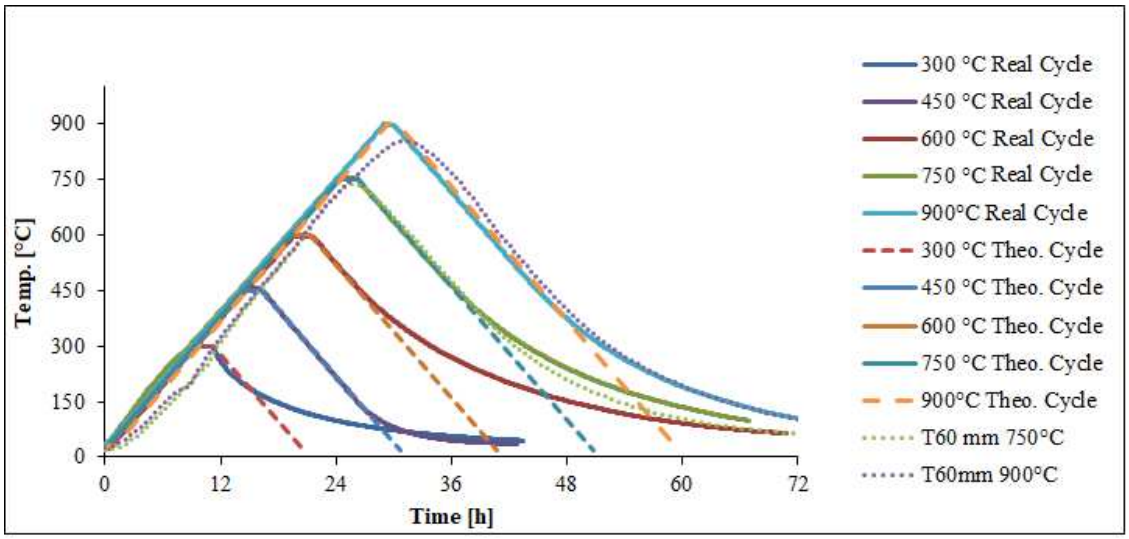

Figure 7 Temperature time histories of the different heating–cooling cycles before characterisation tests

The slow heating tests were conducted in an electrical 1100 × 1200 × 1100 mm furnace. Type K thermocouples were used to monitor the temperatures inside (embedded thermocouple at mid-height and mid-diameter of the concrete cylinder) and on the surface of the specimens, as well as the air temperature in the furnace.

Gas permeability (k_a): The permeability was measured using a Cembureau permeameter with nitrogen as the neutral gas. Concrete specimens (diameter 150 mm × height 35 mm) were subjected to a constant upstream pressure. Gas was injected at the lower surface of the specimen. The injection pressure was applied and maintained until gas flow stabilisation through the material. The pressure and flow rate were recorded during the tests. The downstream pressure was the atmospheric pressure. The front and back pressures of the specimen were measured using thermal mass flow meters with different capacities. This allowed for the mass flow rate to be converted to an equivalent volumetric flow rate. Applying the principle of mass conservation to Darcy's law for the isothermal flow of a gas, considered perfect, enables the apparent permeability, k_a (m^2), to be determined [41].

The apparent permeability was calculated using the following equation:

$$K_a = \frac{2 \times \mu \times Q \times l \times P_{atm}}{A(P_1^2 - P_{atm}^2)}, \quad (1)$$

where μ is the nitrogen (N_2) dynamic viscosity *[Pa·s]*, Q is the volume flow rate *[m^3/s]*, P_{atm} is the atmospheric pressure *[Pa]*, l is the thickness of the specimen *[m]*, A is the section of the specimen *[m^2]*, and P_1 is the absolute gas pressure at the inlet of the specimen *[Pa]*.

The applied absolute gas pressure varied from 1 to 4 bar, depending on the concrete type and deterioration level.

Slices 35 mm thick were sawn from Ø150 × 300 mm concrete cylinders. Permeability measurements were conducted in an air-conditioned room (20 ± 1 °C). Each slice was tested at five different injection pressures.

Modulus of elasticity (E): Three Ø150 × 300 mm cylindrical specimens were tested for each mixture and each heating–cooling cycle. The specimens were subjected to three loading–unloading cycles with 20 s of rest during the compression test. The loading rate was 0.5 $MPa \cdot s^{-1}$ according to NF EN 12390-13 [42].

Compressive strength (fc): Four Ø150 × 300 mm cylindrical concrete specimens were tested for each mixture and each heating–cooling cycle. The imposed stress during uniaxial compressive loading was 0.5 $MPa \cdot s^{-1}$ on an INSTRON 3000 kN hydraulic press according to the European standard [43].

1.4.4 Measurement of thermal properties during heating

Thermal properties (λ, a, c_p): The thermal conductivity and specific heat were measured at high temperatures using Hot Disk probe TPS1500 equipment. The thermal diffusivity was deduced from the measurements of the conductivity and specific heat. This method is based on the use of a planar probe with transient heating technology. A mica probe with a radius of 14.61 mm and a very fine nickel double spiral (thickness 10 µm) covered with two thin layers of electrically insulating materials were placed between two symmetrical halves of the concrete cylinder slices (diameter 150 mm × height 350 mm). Each specimen must have a flat surface to avoid contact defects with the sensor.

Halves of cylinder slices were pre-dried at 80 °C until a constant mass was obtained, and then heated in a 5-L electric oven controlled using the Hot Disk software. The heating rate was 0.5 °C/min. For each target temperature up to 600 °C, measurements were recorded under isothermal conditions after waiting for the furnace and sensor temperature to stabilise (a variation of less of 0.1 °C during 30 min). The isothermal holding period before the measurement depends on the physico-chemical reactions of the concrete hydrate decomposition, portlandite dihydroxylation, and calcite decarbonation.

2. Results and discussion

The physical characteristics of the fresh and hardened concretes before and after heating are presented in Table 4. Before analysis of the spalling differences, the evolutions of the thermal properties and gas permeability of the different concrete mixtures are described as functions of the temperature. The evolution of the residual mechanical properties is also presented. The spalling and different degradation features are compared for the same mix design as a function of the heating rate (10 °C/min or ISO 834 fire) and the geometry of the specimens. Finally, the temperatures and pressures monitored at different depths in the slab during heating at 10 °C/min allows for the influence of the fibre type on the main factors causing spalling to be analysed. Results showing the residual behaviours of the concretes under different heating conditions are discussed. The discussion focuses on the spalling mechanisms and the influence of polypropylene and steel fibres on the concrete behaviour at high temperature.

Table 4 Physical characteristics of fresh and hardened concretes before and after heating

Concretes	*Bulk density at 90 d [kg/m³]*	*Bulk density after 600 °C heating [kg/m³]*	*Entrained air in fresh concrete [%]*	*Total porosity before heating [%]*	*Total porosity after 500 °C heating [%]*	*Moisture content in weight before heating [%]*
Cref	2336 ± 3.0	2166 ± 8.4	2.8	11.2 ± 0.9	15.6 ± 0.6	4.7 ± 0.4
CS 60	2437 ± 2.1	2238 ± 3.2	2.2	8.5 + 0.2	14.0 ± 0.4	4.5 ± 0.5
CPPS 0.75-60	2447 ± 0.5	2281 ± 12.0	2.4	8.6 + 0.3	14.3 ± 0.4	4.7 ± 0.2

2.1 Evolution of the transfer and residual mechanical properties as a function of the temperature

2.1.1 Transfer properties

2.1.1.1 Gas permeability

Figure 8 shows the evolution of the intrinsic residual permeability of the Cref, CS 60, and CPPS 0.75-60 concretes after heat treatment at 0.5 °C/min. At 80 °C, the gas permeability values were similar for all the mixtures ($k_{int\ Cref} = 4.5 \times 10^{-17}$ m², $k_{int\ CS60} = 2.9 \times 10^{-17}$ m², $k_{int\ CPPS\ 0,75\text{-}60} = 4.5 \times 10^{-17}$ m²). The evolutions of CS 60 and Cref permeabilities at 200 °C were not significant (5.8×10^{-17} m² and 5.9×10^{-17} m², respectively). However, the CPPS 0.75-60

permeability increased rapidly (21 × 10^{-17} m^2). At 500 °C, the CS 60 concrete exhibited a slightly lower permeability than the two other concretes ($k_{int\ Cref}$ = 120 × 10^{-17} m^2, $k_{int\ CS60}$ = 110 × 10^{-17} m^2, $k_{int\ CPPS\ 0,75\text{-}60}$ = 120 × 10^{-17} m^2).

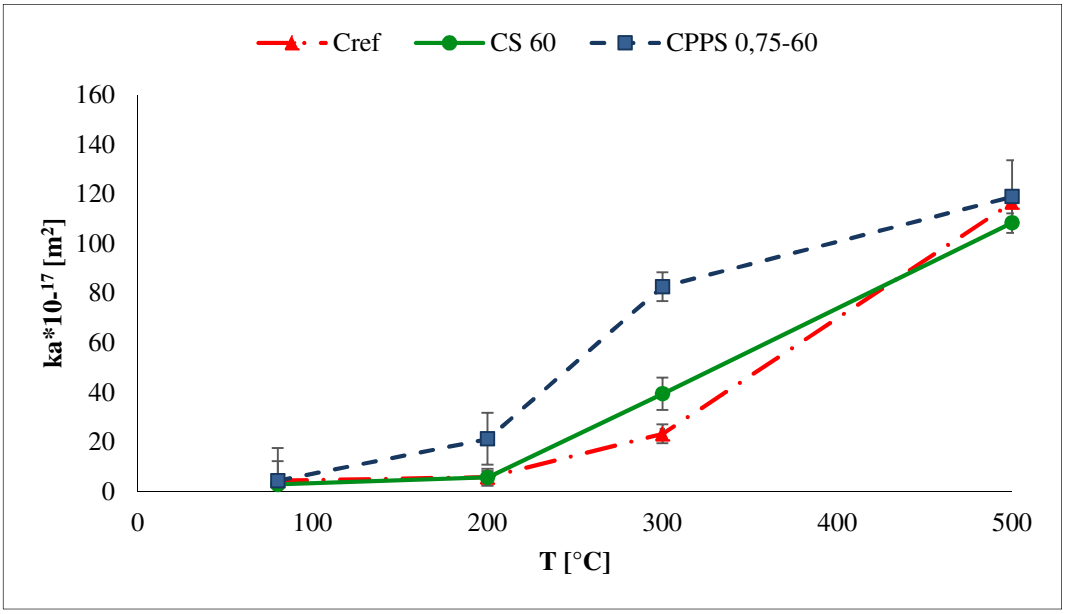

Figure 8 Residual permeability (×10^{-17} m^2) as a function of the heating temperature (T)

The generation of large pores connected by micro-cracks due to the melting of polypropylene fibres created a leakage path that increased the permeability for the CPPS 0.75-60 concrete [5]. This increased permeability occurred at 300 °C for the CPPS 0.75-60 concrete, whereas for the CS 60 and Cref concretes, the increase in permeability, which was only related to cracking induced by the paste/aggregate thermal mismatch, occurred at higher temperatures between 300 °C and 450 °C.

The CS 60 and Cref concretes exhibited similar permeability values.

2.1.1.2 Thermal properties

Thermal conductivity

Figure 9 shows the evolution of the thermal conductivity of the three mixtures (Cref, CPPS 0.75-60, and CS 60) compared to the upper and lower limits of the Eurocode 2 [44] curves as a function of the temperature during heating and cooling.

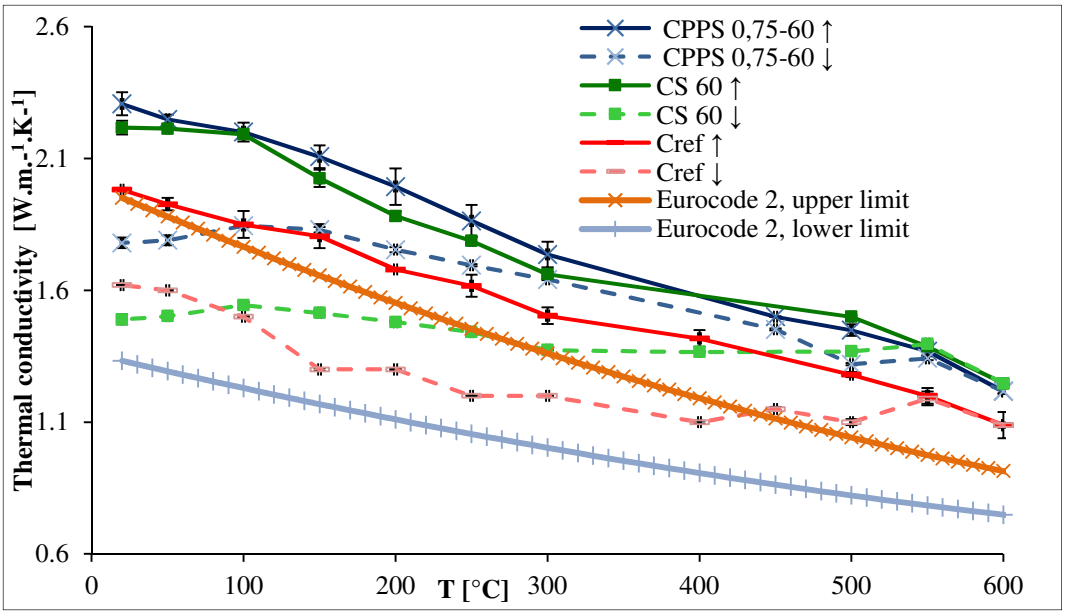

Figure 9 Thermal conductivity ($W \cdot m^{-1} \cdot K^{-1}$) evolution in the Cref, CS 60, and CPPS 0.75-60 concretes compared to the Eurocode 2 [40] curve as a function of the temperature (T) during heating (↑) and cooling (↓)

At 20 °C, the conductivity values for the CS 60 and CPPS 0.75-60 concretes were relatively similar (2.2 and 2.3 $W \cdot m^{-1} \cdot K^{-1}$, respectively), while the conductivity of the Cref concrete was lower (2 $W \cdot m^{-1} \cdot K^{-1}$). From one side, the lower porosity of the CS 60 and CPPS 0.75-60 concretes ($P_{Cref\ 80°C}$ = 11.2%, $P_{CS60\ 80°C}$ = 8.5%, $P_{CPPS\ 0.75\text{-}60\ 80°C}$ = 8.6%) could explain this difference in the thermal conductivity at 20 °C. Bouziadi et al. and Li et al. [45,46] showed that the thermal conductivity of steel fibre (around 50 W/m/°C) is higher than that of the concrete material (less than 2 W/m/°C), which can explain the conductivity difference between Cref and the concretes containing steel fibres.

The thermal conductivity decreased gradually with increasing temperature: the values at 600 °C are 1.1, 1.2, and 1.2 $W \cdot m^{-1} \cdot K^{-1}$ for Cref, CS 60, and CPPS 0.75-60 concretes, respectively. During the cooling period, the thermal conductivity increased slightly, showing hysteresis. This was due to irreversible reactions including the departure of physically and chemically bound water and the appearance of micro-cracks at temperatures above 300 °C. In non-metallic materials, the thermal conductivity is linked to phonon scattering. The phonon collision quantity (thermal vibration) increases with heating. This leads to a reduction in the mean free path of a phonon at high temperature, thus reducing the conductivity. In contrast, during the cooling stage, the increase in conductivity was due to the decrease in phonon collision quantity.

The decrease in thermal conductivity during heating is also partly due to the increase in total porosity and the loss of water during thermal loading.

The upper and lower limits for the thermal conductivity given by Eurocode 2 [44] measured during heating were positioned below the thermal conductivities of the three tested concretes. Nguyen [47] also concluded that the Eurocode seemed to underestimate the thermal conductivity of dried concrete.

Specific heat

Because the specimens should reach thermal equilibrium before measurement, the influence of different physico-chemical transformations on the specific heat could not be determined during these measurements. The specific heat measured in this study should thus be regarded as a fundamental specific heat, which does not consider the latent heat of different physico-chemical transformations.

Figure 10 shows the evolution of the specific heat of the Cref, CS 60, and CPPS 0.75-60 concretes compared to the Eurocode 2 [44] curve as a function of the temperature. The specific heats of the three tested concretes increased with the temperature.

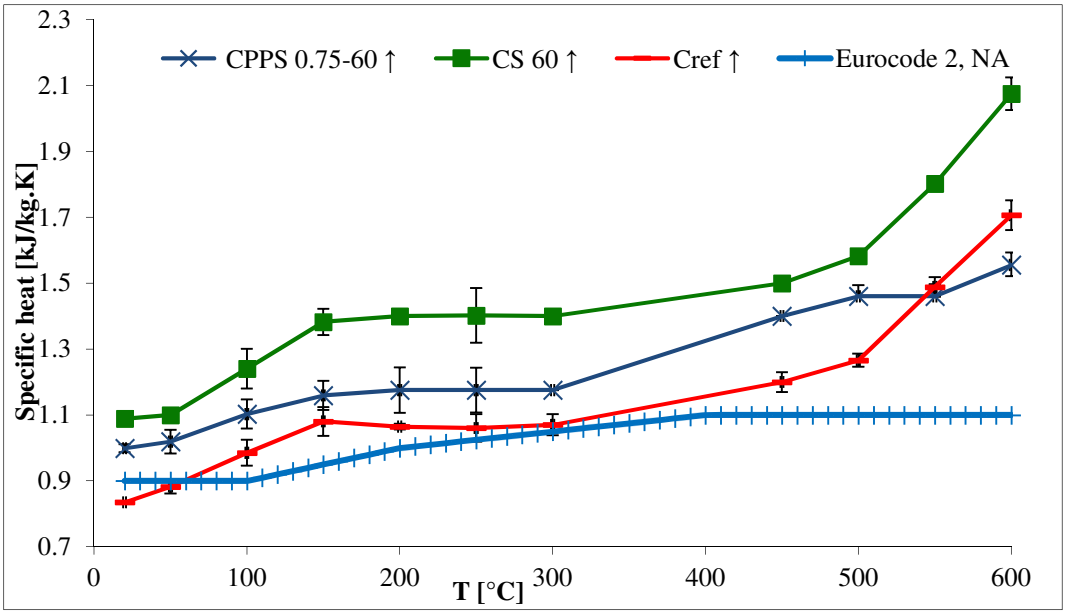

Figure 10 Specific heats (kJ/kg·K) of Cref, CS 60, and CPPS 0.75-60 concretes compared to the Eurocode 2 [44] curve as a function of temperature (T) during heating (↑) and cooling (↓). The maximum standard specific heat deviation is 0.1.

The specific heat increased rapidly between room temperature and 150 °C, after which the increase was slow up to 500 °C. Between 500 °C and 600 °C, the specific heat began to increase more rapidly. Khaliq and Kodur [48] showed the same trend with temperature for a plain concrete and a concrete containing fibres.

The specific heat values were measured under isothermal conditions, and specimens achieved hydrothermal equilibrium before measurement. It should also be noted that the samples were pre-dried before the tests. The measured specific heat should thus be regarded as a fundamental specific heat, which does not consider the latent heat of different physico-chemical transformations. The specific heat is strongly dependent on atomic vibration, which is the main mode of absorption of thermal energy in solids. As the temperature increases, the average atomic vibration energy increases, thus leading to higher values of the specific heat.

The increase in the specific heat was also caused by an increasing porosity within the cement paste. This increase in porosity involves a higher air volume with a slightly higher specific heat (1.0 $kJ \cdot kg^{-1} \cdot K^{-1}$) than that of the concrete (0.9 $kJ \cdot kg^{-1} \cdot K^{-1}$).

The specific heats of the CS 60 and CPPS 0.75-60 concretes were slightly higher than that of the reference concrete (Cref) at room temperature ($Cp_{CPPS\ 0.75\text{-}60}$ = 1.0 $kJ \cdot kg^{-1} \cdot K^{-1}$, $Cp_{CS\ 60}$ = 1.1 $kJ \cdot kg^{-1} \cdot K^{-1}$, Cp_{Cref} = 0.8 $kJ \cdot kg^{-1} \cdot K^{-1}$).

The specific heat curve from Eurocode 2 [44] was positioned below those of the three tested concretes at temperatures above 150 °C.

Thermal diffusivity

Figure 11 shows the evolution of the thermal diffusivity of the Cref, CS 60, and CPPS 0.75-60 concretes from room temperature to 600 °C and from 600 °C back to room temperature.

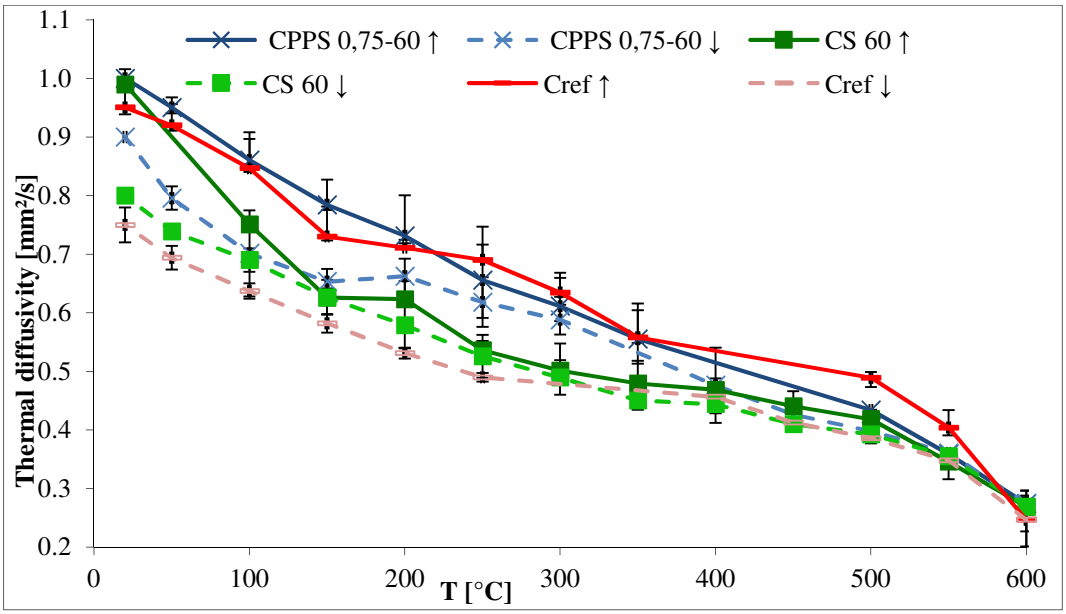

Figure 11 Thermal diffusivities (mm^2/s) of Cref, CS 60, and CPPS 0.75-60 concretes as a function of temperature (T)

For the three different concretes, the thermal diffusivity decreased gradually with heating. Previous studies by Jansson [49], Kodur [50], and Bamonte [51] showed that the decrease in diffusivity was related to the decrease in the density and conductivity and increase in the specific heat.

Unlike the thermal conductivity, the thermal diffusivities of the CS 60 and CPPS 0.75-60 concretes did not exhibit similar evolutions. The CS 60 concrete diffusivity had a greater decrease between 20 °C and 150 °C than the CPPS 0.75-60 concrete. This was related to the higher increase in the specific heat of this concrete over the same temperature range.

For the three mixtures, at 600 °C, the thermal diffusivity lost approximately 75% of its initial value. The Cref and CPPS 0.75-60 concretes showed very similar evolutions of the diffusivity with temperature.

2.1.2 Residual mechanical properties

The mechanical tests at 28 d showed compressive strength values of 60 MPa for the Cref concrete and 80 MPa for the CS 60 and CPPS 0.75-60 concretes. As previous studies have shown that 0.75 kg/m^3 of polypropylene fibres does not affect the evolution of the mechanical

properties with temperature [52], it can be considered that the CS 60 and CPPS 0.75-60 concretes have similar mechanical behaviours.

Mechanical tests were performed on Cref and CPPS 0.75-60 concretes after cooling, to evaluate the influence of the addition of PPF and SF on the mechanical properties after exposure to high temperatures. The mechanical properties of Cref and CPPS 0.75-60 concretes were presented in a previous study [5].

Figure 12 shows the evolution of the absolute residual compressive strength for the Cref and CPPS 0.75-60 concretes.

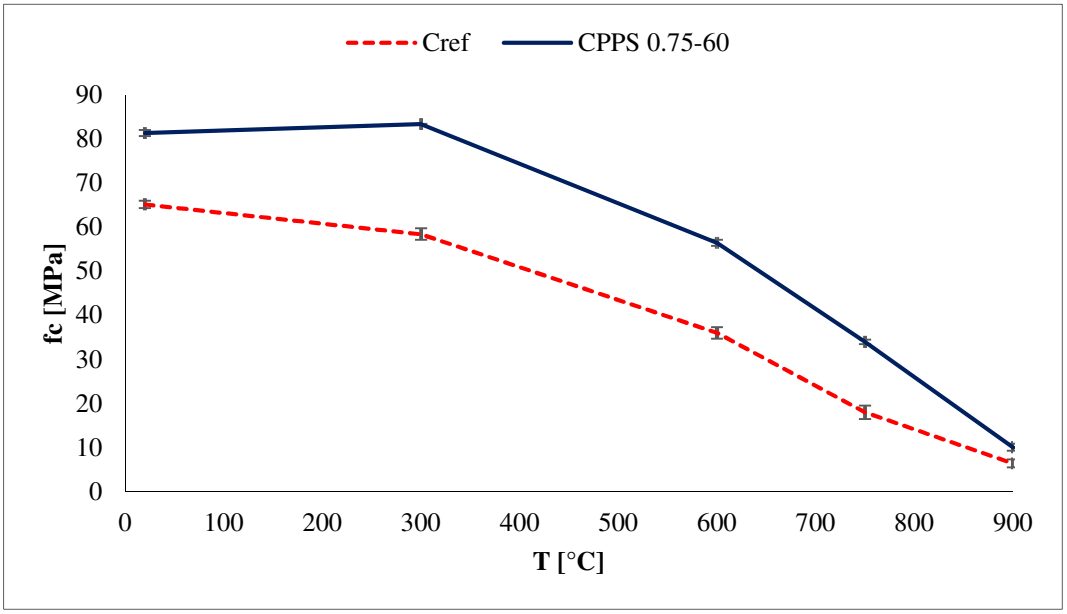

Figure 12 Residual compressive strengths of Cref and CPPS 0.75-60 concretes as a function of temperature

The compressive strength strongly decreased above 300 °C. This was related to the thermal strain mismatch between the aggregate (expanding) and cement paste (shrinkage), which led to tangential and radial cracks at the paste–aggregate interface [53–55].

The most important improvement (approximately 15%) resulting from the addition of the steel fibres to the residual compressive strength was observed between 600 °C and 750 °C. This demonstrates that steel fibres reduced the damage level of the CPPS 0.75-60 concrete.

Figure 13 presents the relative residual compressive strength of the Cref and CPPS 0.75-60 concretes compared to the ACI [56] and EC 4 [57] standards for unstressed specimens after cooling as a function of the temperature. The CPPS 0.75-60 concrete retained a relative compressive strength above the standard curves. The Cref concrete globally fit the EC 4 calcareous curve.

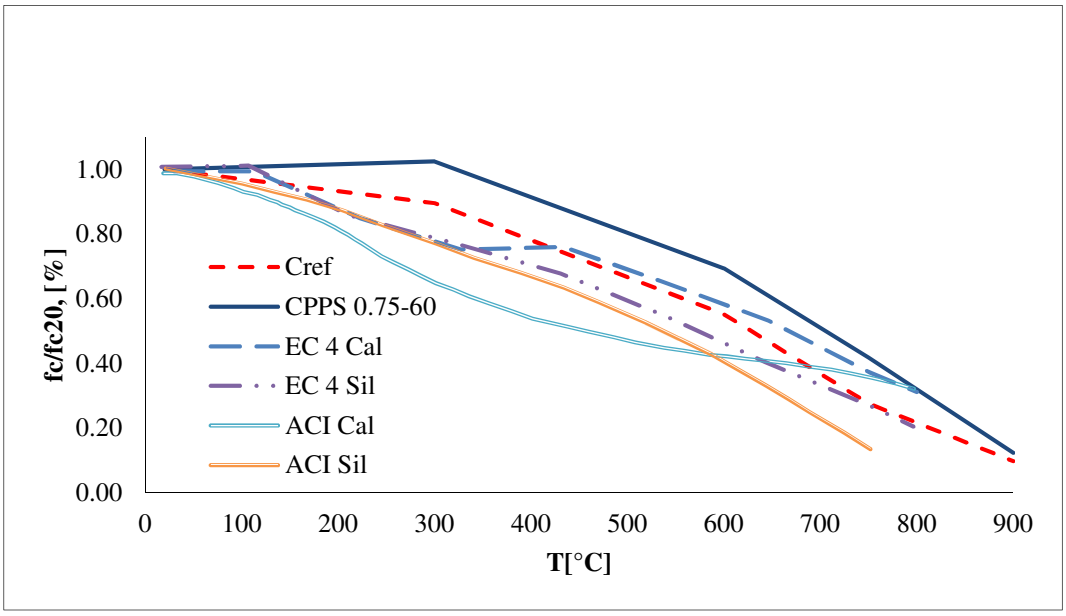

Figure 13 Relative residual (after cooling) compressive strengths of Cref and CPPS 0.75-60 concretes compared to ACI [56] and EC 4 [57] standards as a function of temperature

Figure 14 shows the evolution of the residual modulus of elasticity of the Cref and CPPS 0.75-60 concretes with temperature. The modulus of elasticity of both concretes decreased gradually with increasing temperature. At room temperature, the Young's modulus of CPPS 0.75-60 was 5 GPa higher than that of the Cref. The decrease in the modulus of elasticity was more rapid than that of the compressive strength, up to 30%–35% of the initial values at 600 °C for the Cref and CPPS 0.75-60 concretes, respectively. The reduction in the residual modulus of elasticity was lower for CPPS 0.75-60 concrete than for Cref concrete.

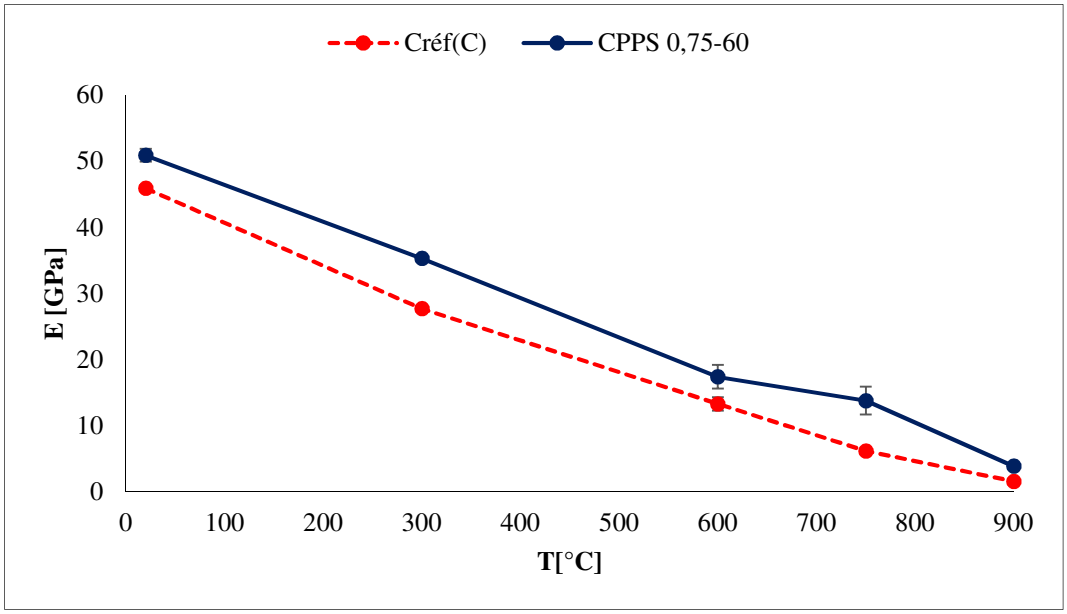

Figure 14 Residual modulus of elasticity of the Cref and CPPS 0.75-60 concretes as a function of the temperature (T)

From 20 °C to 750 °C, the relative modulus of elasticity of the CPPS 0.75-60 concrete showed an average improvement of 8% compared to the Cref concrete.

At 900 °C, the modulus of elasticity values were low. A similar behaviour in the residual compressive strength evolution was observed by Ezziane et al. [58]. The authors attributed this behaviour to the oxidation (500 °C) and subsequent corrosion (700 °C) of the steel fibres.

Globally, the residual mechanical properties of the CPPS 0.75-60 concretes were higher than those of the Cref concretes, confirming the contribution of steel fibres for controlling thermal cracking and limiting the spread of cracking during mechanical testing.

2.2 Depth, surface, and volume of spalled concrete for different geometries and thermal loading

An ISO 834 fire test and a heating test at 10°C/min in which cylindrical specimens and slabs for the three concrete mixtures were heated to 600 °C, were performed to investigate the effects of the heating rate and specimen geometry on concrete spalling. There was no spalling observed on concretes during heating at 0.5 °C/min. The spalling details after the ISO 834 fire test and heating at 10 °C/min are listed in Table 5.

Table 5 Spalling volume, surface, and depth on Cref, CS 60, and CPPS 0.75-60 concretes for different heating rates and specimen geometries

Concretes	**Heating rates**	**Shapes (mm)**	**Spalling volume (%)**	**Spalling surface (%)**	**Max spalling depth (cm)**	**Number of spalled specimens/total number of specimens**	**Moisture content (%)**
Cref	ISO 834 fire (1100 °C)	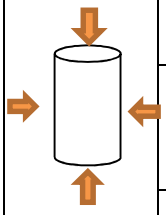 150 × 300	-	-	-	0/26	4.7
CS 60			Not measured	27.0 ± 3.5	3.0 ± 0.7	9/9	4.5
CPPS 0.75-60			-	-	-	0/9	4.7
Cref	10 °C/min, 600 °C	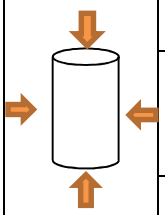 150 × 300	Explosive spalling	Explosive spalling	Explosive spalling	4/4	4.9
CS 60			Not measured	75.0 ± 7.8	5.0 ± 1.2	4/4	5.2
CPPS 0.75-60			-	-	-	0/4	4.1
Cref	10 °C/min,	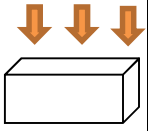	5.0	42.0	3.0	1/2	3.7
CS 60			10.0	64.0	3.0	2/2	3.2

CPPS 0.75-60	600 °C	600 × 300 × 120	-	-	-	0/2	3.5

Thermal stability of Cref concrete

After the ISO 834 fire test, the Cref concrete did not exhibit any spalling (Table 6). The Cref concrete cylinders exhibited explosive spalling during heating at 10 °C/min (Table 6). The sloughing-off of large pieces can be attributed to sudden failure with a large release of energy. The Cref concrete slab also spalled during heating at 10 °C/min. Small pieces of concrete fell off the surface of the slab, showing a progressive spalling behaviour. The spalling volume represented 5% of the total volume, and the spalling surface was 42% of the heated surface (Table 5). The maximum spalling depth was approximately 3 cm. The spalling was more severe in the concrete cylinders than the slabs. The one-side heating of the slabs allows vapour and liquid water to migrate out from the specimen, which limits the risk of spalling.

The Cref concrete slab and cylinders heated at 10 °C/min showed spalling volumes of 5% and a spalling surface of 42% (Table 7). The maximum spalling depth was approximately 3 cm. The one-sided heating seems logically more favourable than multi-directional heating.

Table 6 Cylinders of Cref, CS 60, and CPPS 0.75-60 concretes after ISO 834 and 10 °C/min heating tests

Concrete	**Concrete specimen after heating**	
	ISO 834 fire	**10 °C/min**

Cref		 
CS 60		 
CPPS 0.75-60		

Table 7 Heated surface of the concrete slabs after heating at 10 °C/min to 600 °C

Type of concrete mix	**Concrete after heating at 10 °C/min**
Cref	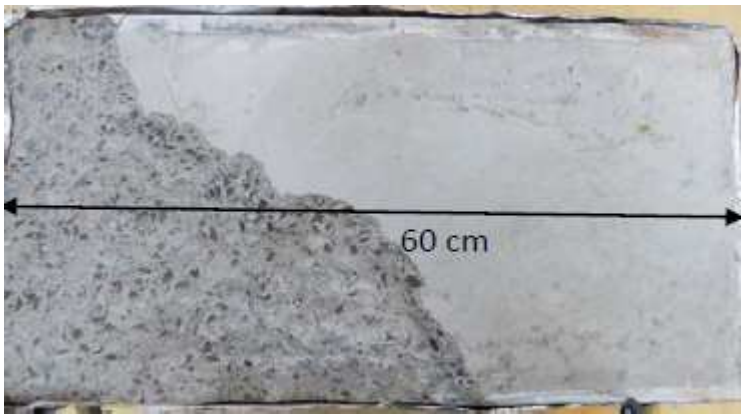
CS 60	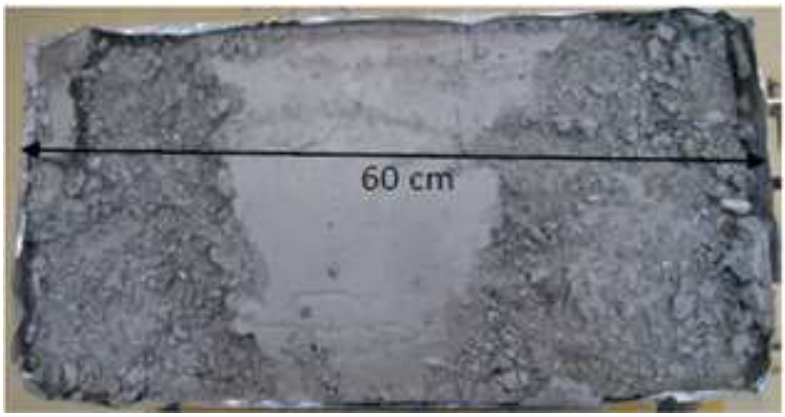
CPPS 0.75-60	

Thermal stability of CS 60 concrete

The CS 60 concrete cylindrical specimens exposed to ISO 834 fire conditions showed surface spalling after 24 min of heating and a surface temperature of 850 °C (Table 6). The maximum

total spalling surface was approximately 27% of the exposed surface and the maximum total spalling depth was 3 cm. A reduction in the mechanical properties of the steel fibres was observed after cooling.

During heating at 10 °C/min, the four CS 60 concrete cylindrical specimens spalled covering up to 75% of the total surface with a maximum spalling depth of 5 cm (Table 5 and Table 6). The falling off of small pieces can be attributed to a progressive surface spalling behaviour. The amount of spalling on the CS 60 concrete cylinders was higher for heating at 10 °C/min to 600 °C than for the ISO 834 fire conditions.

The spalling phenomena on the CS 60 concrete cylinders was less severe for the ISO 834 fire test than for heating at 10 °C/min.

The CS 60 concrete slab heated at 10 °C/min also suffered spalling and exhibited more damage than the Cref concrete slab. Its spalling volume percentage was 10%, spalling surface percentage was 64%, and maximum spalling depth was approximately 3 cm (Table 5 and Table 7).

The occurrence of spalling in concrete containing steel fibres was also reported by Chen and Liu [34]. Heating tests at 10 °C/min for concrete cubes with 48 kg/m^3 of steel fibres showed severe spalling after heating to 800 °C. The residual compressive strength of the concretes was 82 MPa.

Thermal stability of CPPS 0.75-60 concrete

The CPPS 0.75-60 concrete did not experience any pieces falling off during the different heating scenarios (Table 6 and Table 7). As for the cylindrical specimens, the CPPS 0.75-60 concrete slab presented in Table 6 also did not exhibit spalling. The polypropylene-and-steel fibre mixture appears to be an effective solution for limiting explosive spalling.

In summary, the results showed that spalling occurred for CS 60 concrete regardless of the specimen geometry and the boundary thermal conditions. Conversely, the CPPS 0.75-60 concrete did not exhibit any spalling, regardless of the heating conditions. No spalling of the Cref concrete specimens occurred during the ISO 834 fire test; however, with heating at 10 °C/min, cylindrical specimens of Cref concrete exploded and the slab specimen exhibited surface spalling. When heated at 10 °C/min, surface spalling was observed on CS 60 concrete cylinders, while Cref cylinders exhibited explosive spalling, leading to concrete being broken off in several pieces. This difference in the spalling behaviour highlights the influence of steel fibres on the spalling process at 10 °C/min and spalling occurrence under the ISO 834 fire

test. For all the concrete mix designs, the unidirectional thermal loading appears more favourable than heating on all sides at 10 °C/min.

2.3 Temperature and pore pressure evolution within concrete slabs

2.3.1 Temperature evolution within concrete slabs during heating at 10 °C/min

Figure 15 shows the temperature evolution at different depths (5 mm, 30 mm, and 60 mm from the heated slab surface) and on the unexposed surface. Thermocouples located 30 mm below the heated surface of the Cref and CS 60 concrete slabs broke down following spalling events, and their values have not been plotted in the figure. Two thermocouples placed on the heated surface (Tsurf1, Tsurf2) of each slab demonstrated that the temperature distribution was homogeneous over the entire exposed section. The surface temperature evolution of the Cref and CS 60 concretes showed disruption characterised by a sudden temperature decrease and growth. The decrease was identified at Tsurf = 500 °C for the CS 60 concrete and Tsurf = 500–600 °C for the Cref concrete. This sudden change in temperature could indicate the occurrence of spalling. The 60 mm thermocouple in the CS 60 concrete reached a plateau, and the temperature remained almost constant for a few minutes (Figure 16). This plateau at a local temperature of 130 °C can be attributed to the endothermic nature of water vaporisation. Vaporisation consumes a significant amount of energy, thereby reducing the amount of heat transfer. This plateau in the time–temperature curve at a depth of 60 mm was smaller for the Cref concrete and did not appear for the CPPS 0.75-60 concrete (Figure 16). This is probably due to thermal cracking inside the concrete, which allows for more moisture loss during the test. Therefore, the clear plateau observed in the CS60 concrete indicates a greater difficulty of water escaping from the CS 60 concrete. However, the gas permeability results do not seem to corroborate this hypothesis: after heating at 300 °C, the permeability value for the CS 60 concrete was between that of the Cref and CPPS 0.75-60 concretes. However, in a previous study, mercury porosity measurements [5] showed that the presence of steel fibres impacted the porous network structure at high temperatures (200–500 °C). The steel fibres seemed to limit the appearance of new large pores (1 µm to 10 µm). Further measurements of permeability in the temperature range of 100–200 °C would be necessary to confirm or refute this hypothesis.

The higher temperatures observed for the CS 60 concrete could be related to the spalling and consequent decrease of the concrete thickness covering the thermocouple (Figure 1

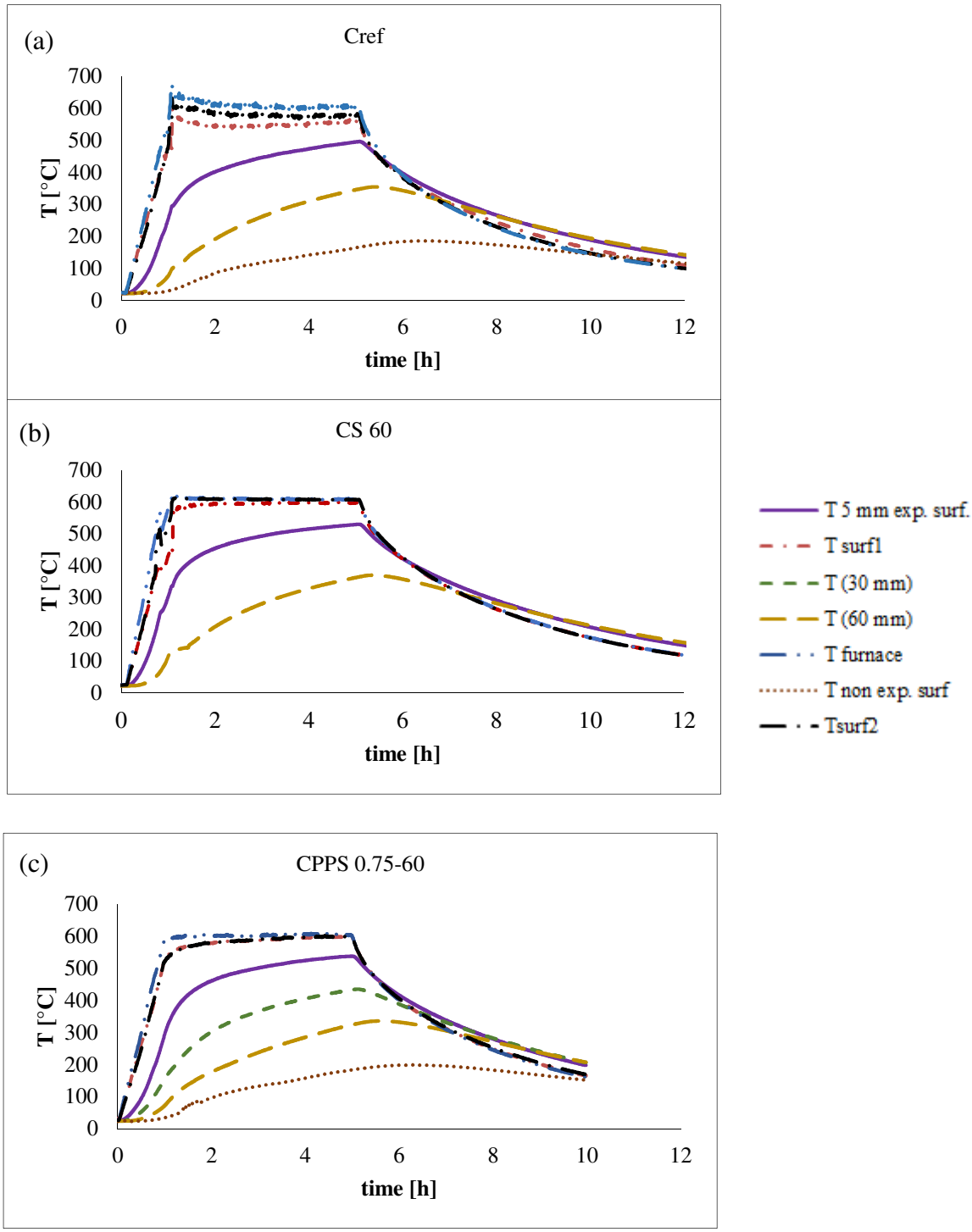

Figure 15 Temperature evolution as a function of time at different depths in the (a) Cref, (b) CS 60, and (c) CPPS 0.75-60 concrete slabs

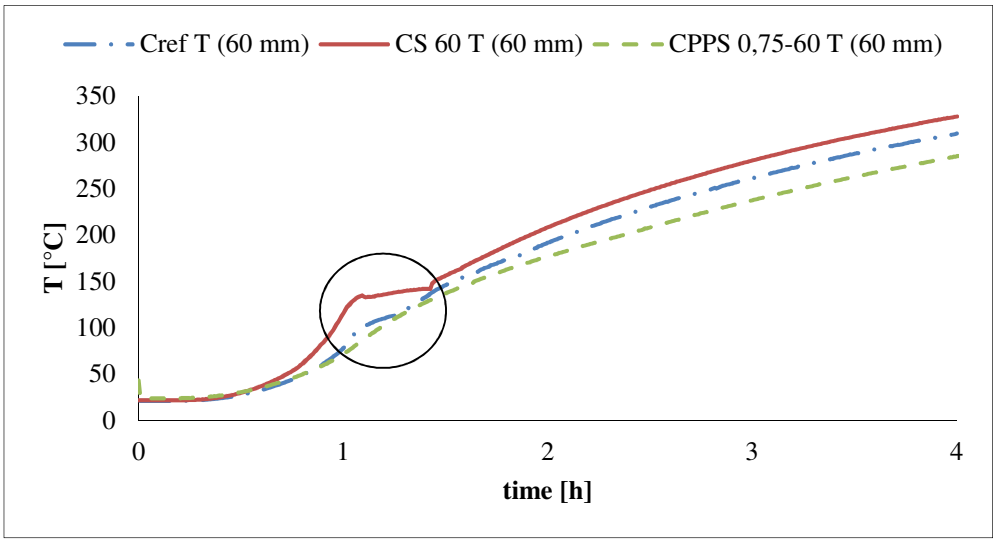

Figure 14 Temperature evolution at depths of 30 and 60 mm below the heating surface during the first 4 h for Cref, CS 60, and CPPS 0.75-60 concrete slabs

2.3.2 Pore pressure evolution within concrete slabs

Figure 17 shows the evolution of the pressures and temperatures measured at a depth of 60 mm as a function of time. Generally, the pressure increased rapidly to a maximum value and then decreased gradually. The curve for the CPPS 0.75-60 concrete did not show a consistent evolution compared to the physical phenomenon. It is possible that the measurement was disrupted by local cracking or a sensor malfunction. The maximum pore pressures within the CS 60 and Cref concretes occurred at the same time and was consistent with the same increase in temperature with time observed in the different concretes (Figure 15, Figure 17).

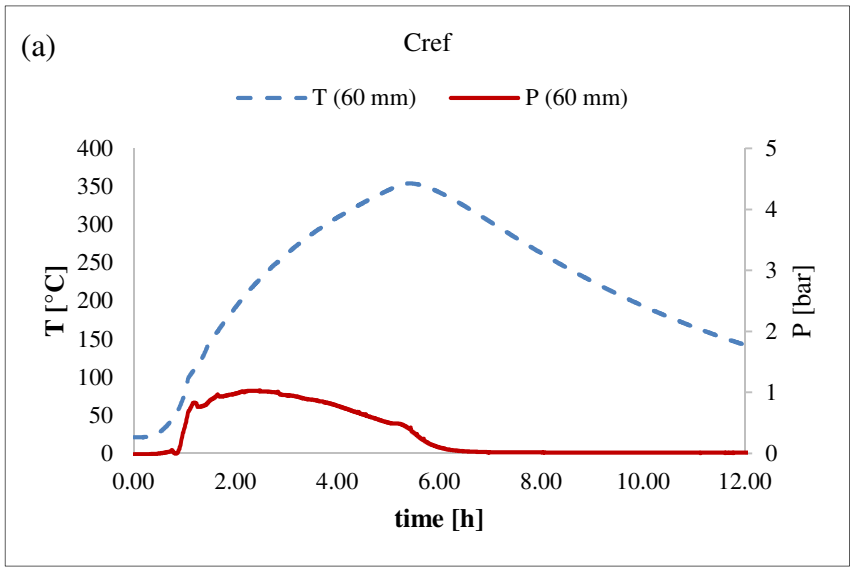

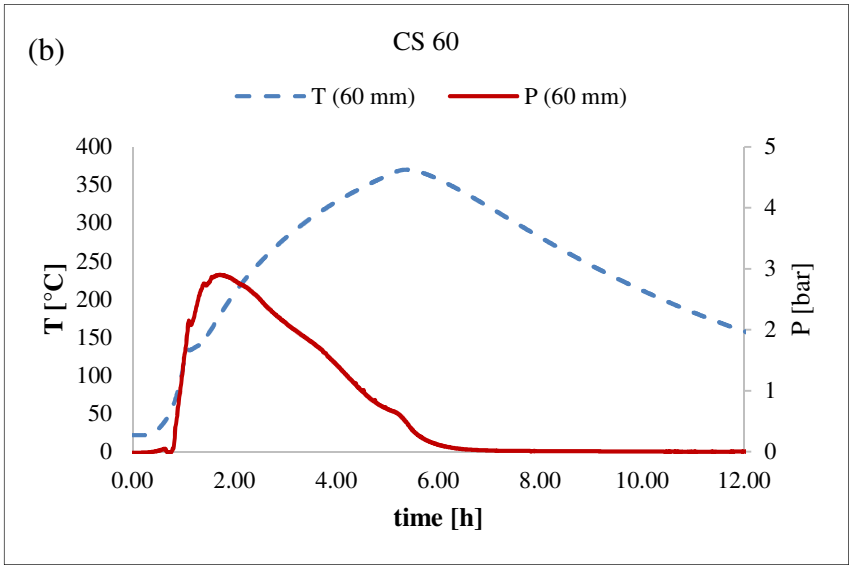

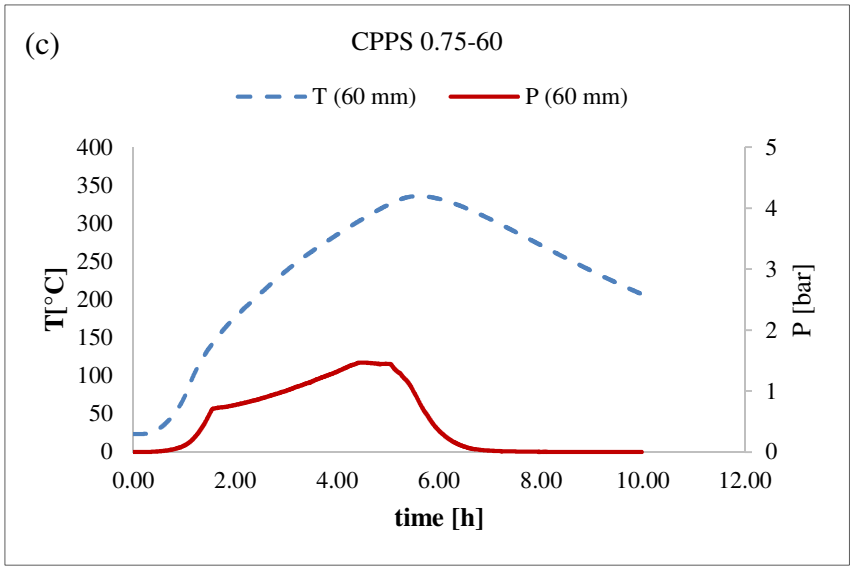

Figure 17 Temperature and pressure evolutions in the (a) Cref, (b) CS 60, and (c) CPPS 0.75-60 concretes at a depth of 60 mm as a function of time

It is important to note that the pressures measured at a depth of 60 mm did not necessarily match the value of the maximum pressure developed in the concrete. The recorded maximum pressure at 60 mm was 2.9 bar at a local temperature of 220 °C. The pressure increase

followed the water departure. The recorded pore pressure was higher within the CS 60 concrete slab. This could be related to a more difficult evacuation of water, as noted in the temperature curve (Figure 15). The presence of steel fibres appears to affect the mass transfer and pore pressure evolutions.

Bangi et al. [19] tested a concrete containing a mixture of 0.1% and 0.4% polypropylene and steel fibres, respectively. The concrete with a strength of 71 MPa was heated at 10 °C/min to 600 °C. The pressure was measured at depths of 10, 30, and 50 mm. The maximum pressure did not exceed 10 bar. The results of the present study showed lower values than those reported by Bangi et al. One reason that could explain the difference between these two studies is the curing method: lime-saturated water in Bangi et al. versus plastic bags in our case.

According to Monte et al. [6], the pore pressure values of concrete slabs containing steel fibres are similar to or higher than those for plain concrete. Square slab specimens with side lengths of 800 mm and a thickness of 100–200 mm were subjected to ISO 834 fire heating and to a membrane compression of 10 MPa.

Figure 18 shows the evolution of the temperature difference between the surface and a depth of 60 mm as a function of the temperature at 60 mm. The Cref and CS 60 concrete curves exhibit disruption, which can be explained by the spalling of the surface. The highest temperature difference occurs at a local temperature in the range of 80 °C to 150 °C. Otherwise, the local temperatures corresponding to the highest pore pressure range from 80 °C to 220 °C (Figure 17). For the CS 60 concretes, Figure 17 (b) shows that the pressure increase occurs almost at the beginning of a plateau in the time–temperature curve and the peak was achieved at the end of this plateau. The kinetics of the hygral and thermal processes lead simultaneously to significant magnitudes of the thermal stresses associated with temperature gradients and the stresses induced by pressure. This theory is consistent with the hypothesis in the literature for the double spalling origin [4,59].

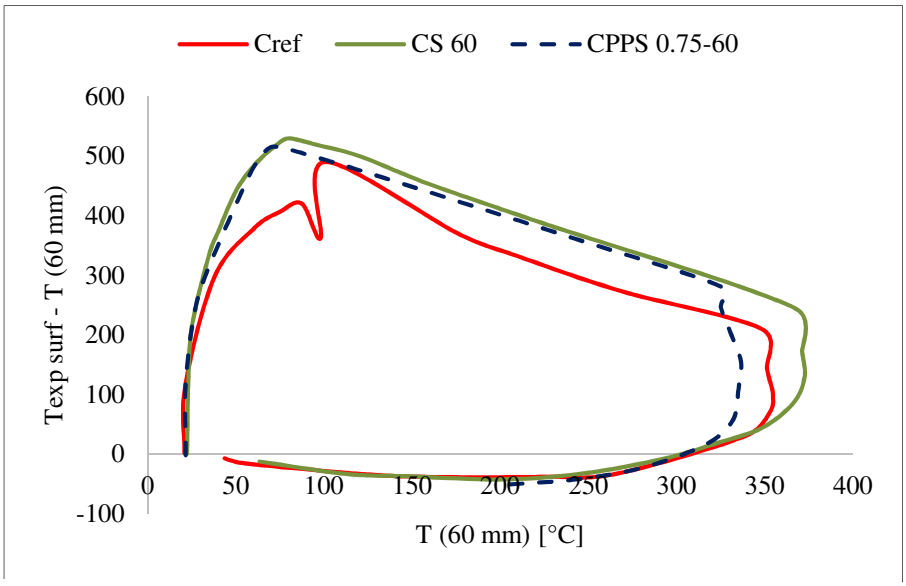

Figure 15 Evolution of the difference in temperature between the surface and a depth of 60 mm as a function of the temperature at 60 mm for Cref, CS 60, and CPPS 0.75-60 concretes

2.4 Discussion

At a heating rate of 10 °C/min, the Cref concrete cylinders showed explosive spalling, while one of the two slabs showed surface spalling. However, the Cref concrete cylindrical specimens did not spall under ISO fire conditions. A rapid increase of the temperature generates a higher thermal gradient and higher surface compressive stresses. This phenomenon may induce strong concrete cracking on the peripheral surface of the specimen. These cracks facilitate the evacuation of liquid water and steam toward the outside of the specimen, thus limiting the amount of condensed water that migrates inside the specimen. A decrease in the amount of condensed water reduces the chances of moisture clog formation [10,19]. Felicetti et al. [60] monitored the pore pressure during heating of concrete elements at rates of 120 °C/min, 10 °C/min, and 1 °C/min. The results showed that the highest pore pressure values were obtained for a heating rate of 10 °C/min because cracking induced by thermal stress (in the case of fast heating) and drying due to prolonged vapour flows (in the case of slow heating) lead to significantly lower pressure peaks. Thermally induced cracks tend to enhance gas permeability and pressure release. Spalling observations showed a greater spalling depth in the CS 60 concrete cylinders for heating at 10 °C/min (50 mm) than for the ISO 834 fire test (30 mm).

The difference in the spalling depth can be related to the numerical results reported by Gavin et al. [20], who showed that at slow heating rates, the values of the liquid moisture saturation and vapour pressure are slightly higher than those observed during fast heating, such as under the ISO-834 fire conditions. In addition, at low heating rates, the maximum pressure values occur at a greater distance from the heated surface than in the case of faster heating [20]. The migration of fluid becomes easier, allowing for a decrease in the pore pressure. The polypropylene fibres prevent spalling during one-side heating when thermal stresses play a dominant role, but they also prevent the spalling of small cylinders heated on all sides where the thermo-hydrous mechanism is dominant.

In this study, no spalling of the CPPS 0.75-60 concrete occurred. This was explained by the influence of the polypropylene fibres on the concrete microstructure. This phenomenon has been previously highlighted by numerous authors [52,61,62]. After the melting of polypropylene fibres (170 °C), the pores become interconnected by a network of micro-cracks, thus creating favourable leakage paths. The greater increase in the CPPS 0.75-60 permeability values between 150 °C and 300 °C compared to that of the other concretes confirms this hypothesis (Figure 8). The easier fluid transport allowed for better drainage. As a result, lower pore pressures could be expected within the concrete; however, the values measured at a depth of 60 mm from the slab surface do not show much difference from those for the Cref concrete (Figure 17). The micro-cracks that opened during heating near the heated side would facilitate the departure of liquid water toward the outside of the specimen. The decreased amount of liquid water reduced the consumption of latent heat due to water vaporisation. Therefore, the thermal gradient within the concrete element would be much lower, leading to a decrease in the thermo-mechanical stresses (Figure 18). Thus, polypropylene fibres would have a favourable impact on both the thermo-hydric process and the thermo-mechanical process. The absence of spalling during one-side heating when thermal stresses play a dominant role on the spalling behaviour, but also the absence of spalling in small cylinders heated on all sides, seem to support this hypothesis.

When steel fibres were added to the concrete, spalling occurred regardless of the boundary thermal conditions, specimen geometry, or heating rates. The results showed the influence of steel fibres for lessening the reduction of residual mechanical properties with increasing temperature. Steel fibres control crack development and prevent the occurrence of large crack widths [5]. During the ISO 834 fire test, the cracking on the CS 60 concrete cylinder surface was not as important as it was for the Cref concrete.

Steel fibres increased the thermal conductivity of the concretes but decreased their specific heat, especially for the CS 60 concretes (Figure 9 and Figure 10). As a result, the thermal diffusivity of the CS 60 concrete was lower than that of the other concretes (Figure 11), which leads to slower heat conduction. A higher thermal gradient could thus have been expected for the CS 60 concrete, but the temperature evolutions within the concrete do not show such a trend. Variations in the slab thickness depending on the spalling amount may impact the temperature distribution within the concretes and make interpretation more difficult. Otherwise, a higher modulus of elasticity leads to higher thermal stresses and increases the spalling sensitivity, as evidenced by the spalling of CS 60 concretes at the higher heating rate (ISO 834). Indeed, spalling can occur when the thermo-mechanical stresses and pore pressure reach certain threshold values. The higher the thermo-mechanical stresses are, the lower the pressure threshold value leading to spalling will be. Steel fibres may also influence the thermo-hydraulic mechanism, as shown by the higher pore pressure value measured in the CS60 concrete compared to that of the other concretes. However, unlike what could be expected, the CS60 concrete did not exhibit lower residual permeability values than the other concretes did. A longer plateau in the time–temperature curve related to heat consumption due to the water phase change could indicate a greater amount of water. Water may have had more difficulty migrating through the CS60 concrete because it was less damaged.

Steel fibres exhibited an influence on the spalling of specimens during heating at 10 °C/min. The Cref cylinders exhibited explosive spalling, whereas the CS 60 cylinders presented surface spalling. Steel fibres, through being pulled out or off of the specimens, absorbed a large quantity of energy and modified the concrete spalling behaviour.

3. Conclusion

This study presents several heating tests (ISO 834 fire test and heating at 10 °C/min) and characterisation tests at a heating rate of 0.5 °C/min for concretes with or without polypropylene and/or steel fibres in order to better understand the influence of these fibres on the concrete spalling behaviour. Some conclusions can be drawn from the results:

- The results show that the addition of polypropylene fibres led to an increase in the residual gas permeability, particularly between 200 °C and 300 °C. The steel fibres led to an increase in the thermal conductivity, but also to an increase in the specific heat.

Steel fibres reduced the loss of mechanical residual properties with increasing temperature.

- The thermal conductivity decreased almost linearly with the temperature between 20 °C and 600 °C. During cooling, there was a slight gain in conductivity. The hysteresis between heating and cooling can be explained by the irreversibility of reactions, such as the departure of physically and chemically bound water and the appearance of micro-cracks above 300 °C, which lead to deterioration of the material. Within the slabs, the pressure and temperature gradients both reached significant values in the same temperature range (80 °C to 220 °C). This indicates that both thermo-mechanical and thermo-hydrous processes were involved in the spalling behaviour.
- Plain concrete (Cref) did not show spalling under the ISO 834 fire test, whereas explosive spalling appeared during heating at 10 °C/min. Faster temperature loading generated a higher thermal gradient and higher surface compressive stresses, which may induce the cracking of the peripheral part. Thus, the evacuation of liquid water and steam to the outside of the concrete was easier. This process also limits the migration of water into the colder inner part of the specimen.
- Spalling was more severe for concrete cylinders than slabs. The one-side heating of the slabs allowed vapour to migrate out from the unexposed part of the specimen. The addition of steel fibres changed the spalling mode of cylindrical specimens from explosive spalling in large pieces (Cref) to surface spalling in small pieces (CS 60).
- The CS 60 concrete exhibited spalling regardless of the type of thermal load (ISO 834 or 10 °C/min) or the boundary thermal conditions (one-side heating or all-side heating). The higher modulus of elasticity of the CS 60 concrete increased the thermo-mechanical stresses during heating. Steel fibres also had an influence on the thermo-hydric process, as shown by the higher pore pressure value measured in the CS60 concrete compared to the other concretes. Furthermore, the influence of steel fibres on limiting the crack widths on the cylinder periphery might explain the occurrence of spalling during the ISO 834 fire test for CS 60 concrete and not Cref concrete.
- The addition of polypropylene fibres (0.75 kg/m^3) to the CS 60 concrete mix was effective in preventing spalling at each heating rate. The positive action of polypropylene fibres was clearly shown by the higher gas permeability of the CPPS 0.75-60 concrete, particularly between 200 °C and 300 °C. The addition of 60 kg/m^3 of steel fibres had an unfavourable influence on spalling, especially under rapid

heating (ISO 834 fire test). Adding 0.75 kg/m^3 of polypropylene fibres to the CS 60 concrete (CPPS 0.75-60) prevented spalling. The CPPS 0.75-60 concrete did not exhibit any spalling. It would be interesting to test different steel fibre contents of less than 60 kg/m^3 to identify the stability threshold and recognise the effects of adding polypropylene fibres based on the case.

Acknowledgments

The authors express their thanks to FNTP (Fédération Nationale des Travaux Publics) and EIFFAGE Génie-Civil for their financial and technical support.

References

[1] P. Kalifa, G. Chéné, C. Gallé, High-temperature behaviour of HPC with polypropylene fibres - From spalling to microstructure, Cem. Concr. Res. 31 (2001) 1487–1499. doi:10.1016/S0008-8846(01)00596-8.

[2] F.-J. Ulm, O. Coussy, Z. Bazant, The "Chunnel fire". I: chemoplastic softening in rapidly heated concrete, J. Eng. Mech. (1999) 272–282.

[3] T. Harmathy, Thermal properties of concrete at elevated temperatures, J. Mater. 120 (1965) 47–74.

[4] G.A. Khoury, Y. Anderberg, Concrete Spalling Review, Fire Saf. Des. 60 (2000) 5–12.

[5] N. Yermak, P. Pliya, A. Beaucour, A. Simon, A. Noumowé, Influence of steel and / or polypropylene fibres on the behaviour of concrete at high temperature : Spalling , transfer and mechanical properties, Constr. Build. Mater. 10 (2017) 240–250. doi:10.1016/j.conbuildmat.2016.11.120.

[6] F. Lo Monte, R. Felicetti, Heated slabs under biaxial compressive loading : a test set-up for the assessment of concrete sensitivity to spalling, Mater. Struct. 50 (2017) 1–12. doi:10.1617/s11527-017-1055-1.

[7] G.H.A. Van der Heijden, R.M.W. Van Bijnen, L. Pel, H.P. Huinink, Moisture transport in heated concrete, as studied by NMR, and its consequences for fire spalling, Cem. Concr. Res. 37 (2007) 894–901. doi:10.1016/j.cemconres.2007.03.004.

[8] G.H.A. Van Der Heijden, L. Pel, O.C.G. Adan, Fire spalling of concrete, as studied by NMR, Cem. Concr. Res. 42 (2012) 265–271. doi:10.1016/j.cemconres.2011.09.014.

[9] F. Lo Monte, P. Gambarova G., Corner spalling and tension stiffening in heat-damaged R / C members : a preliminary investigation, Mater. Struct. (2015) 3657–3673. doi:10.1617/s11527-014-0429-x.

[10] J.-C. Mindeguia, P. Pimienta, H. Carré, C. La Borderie, Experimental analysis of concrete spalling due to fire exposure, Eur. J. Environ. Civ. Eng. 17(6) (2013) 453–466.

[11] P. Kalifa, F.-D. Menneteau, D. Quenard, Spalling and pore pressure in HPC at high temperatures, Cem. Concr. Res. 30 (2000) 1915–1927. doi:10.1016/S0008-8846(00)00384-7.

[12] A. Caggiano, D. Said, G. Etse, M. Ripania, Meso-scale response of concrete under high temperature based on coupled thermo-mechanical and pore-pressure interface modeling, Eng. Fail. Anal. 85 (2018) 167–188. doi:10.1016/j.engfailanal.2017.11.016.

[13] J.-C. Liu, K.H. Tan, Y. Yao, A new perspective on nature of fire-induced spalling in concrete, Constr. Build. Mater. 184 (2018) 581–590. doi:10.1016/J.CONBUILDMAT.2018.06.204.

[14] E. Ouedraogo, S. Djaknoun, B. Uch, Q.T. Nguyen, L. Missemer, A. Miras, Y. Malecot, Development of an experimental apparatus aimed at performing thermal-induced spalling tests based on a propane gas burner through tests on ultra-high performance concrete, Constr. Build. Mater. 247 (2020) 118395. doi:10.1016/J.CONBUILDMAT.2020.118395.

[15] M. Maier, M. Zeiml, R. Lackner, On the effect of pore-space properties and water saturation on explosive spalling of fire-loaded concrete, Constr. Build. Mater. 231 (2020) 117150. doi:10.1016/J.CONBUILDMAT.2019.117150.

[16] S. Werner, A. Rogge, The effect of various fire-exposed surface dimensions on the spalling of concrete specimens, Fire Mater. 39 (2014) 545–556.

[17] L. Bostrom, R. Jansson, Fire spalling of concrete - a practical problem or just of academic interest, in: Spalling Due to Fire Expo., Leipzig, 2015.

[18] M. Çiflikli, M. Sarıdemir, F. Soysat, Adverse effects of high temperatures and freeze-thaw cycles on properties of HFRHSCs containing silica fume and metakaolin, Constr.

Build. Mater. 174 (2018) 507–519. doi:10.1016/J.CONBUILDMAT.2018.04.150.

[19] M. Bangi, T. Horiguchi, Effect of fibre type and geometry on maximum pore pressures in fibre-reinforced high strength concrete at elevated temperatures, Cem. Concr. Res. 42 (2012) 459–466. doi:10.1016/j.cemconres.2011.11.014.

[20] D. Gawin, F. Pesavento, B.A. Schrefler, What physical phenomena can be neglected when modelling concrete at high temperature? A comparative study. Part 1: Physical phenomena and mathematical model, Int. J. Solids Struct. 48 (2011) 1927–1944. doi:10.1016/j.ijsolstr.2011.03.004.

[21] K.D. Hertz, Limits of spalling of fire-exposed concrete, Fire Saf. J. 38 (2003) 103–116.

[22] H. Han Young-Sun, H. Cheon-Goo, K. Kyoung-Min, Combined fiber technique for spalling protection of concrete column, slab and beam in fire, Mater. Struct. 48 (2015) 3377–3390.

[23] L. Boström, U. Wickström, B. Adl-Zarrabi, Effect of specimen size and loading conditions on spalling of concrete, Fire Mater. 31 (2008) 173–186.

[24] R.J. Connolly, The spalling of concrete in Fires, Ph.D thesis, Aston University, 1995.

[25] R. Jansson, L.A. Bostrom, Factors influencing fire spalling of self compacting concrete, Mater. Struct. (2013).

[26] G. Debicki, R. Haniche, F. Delhomme, An experimental method for assessing the spalling sensitivity of concrete mixture submitted to high temperature, Cem. Concr. Compos. 34 (2012) 958–963. doi:10.1016/j.cemconcomp.2012.04.002.

[27] C. Maluk, L. Bisby, G. Terrasi, Effects of polypropylene fibre type on occurenece of heat-induced concrete spalling, in: Concr. Spalling Due to Fire Expo., Patis, 2013: pp. 1–8.

[28] J. Bosnjak, J. Ozbolt, R. Hahn, Cement and Concrete Research Permeability measurement on high strength concrete without and with polypropylene fi bers at elevated temperatures using a new test setup, 53 (2013) 104–111. doi:10.1016/j.cemconres.2013.06.005.

[29] L. Phan, Spalling and mechanical properties of high strength concrete at high temperature, in: Proceeding CONSEC' 07, Tours, 2007: pp. 1595–1608.

[30] M. Ozawa, H. Morimoto, Effects of various fibres on high-temperature spalling in

high-performance concrete, Constr. Build. Mater. 71 (2014) 83–92. doi:10.1016/j.conbuildmat.2014.07.068.

[31] M. Hedayati, M. Soafi, P.A. Mendis, T. Ngo, A comprehensive review of spalling and fire performance of concrete members, Electron. J. Struct. Eng. 15 (2015) 28.

[32] B. Rivaz, Technical performance of reinforced concrete with steel fibers and polymers, Tunnels Ouvrages Souterr. №198. (2006) 367–371.

[33] A. Lau, M. Anson, Effect of high temperatures on high performance steel fibre reinforced concrete, Cem. Concr. Res. 36 (2006) 1698–1707. doi:10.1016/j.cemconres.2006.03.024.

[34] B. Chen, J. Liu, Residual strength of hybrid-fiber-reinforced high-strength concrete after exposure to high temperatures, Cem. Concr. Res. 34 (2004) 1065–1069. doi:10.1016/j.cemconres.2003.11.010.

[35] M.R. Bangi, T. Horiguchi, Pore pressure development in hybrid fibre-reinforced high strength concrete at elevated temperatures, Cem. Concr. Res. 41 (2011) 1150–1156.

[36] G. Peng, W. Yang, J. Zhao, Y. Liu, S. Bian, L. Zhao, Explosive spalling and residual mechanical properties of fiber-toughened high-performance concrete subjected to high temperatures, Cem. Concr. Res. 36 (2006) 723–727. doi:10.1016/j.cemconres.2005.12.014.

[37] A. Caverzan, E. Cadoni, M. di Prisco, Dynamic tensile behaviour of high performance fibre reinforced cementitious composites after high temperature exposure, Mech. Mater. 59 (2013) 87–109. doi:10.1016/j.mechmat.2012.12.006.

[38] F.B. Varona, F.J. Baeza, D. Bru, S. Ivorra, Influence of high temperature on the mechanical properties of hybrid fibre reinforced normal and high strength concrete, Constr. Build. Mater. 159 (2018) 73–82. doi:10.1016/j.conbuildmat.2017.10.129.

[39] NF EN 196-1 AFNOR, Méthodes d'essais des ciments, (2016).

[40] 200-HTC RILEM Recommendations, Recommendation of RILEM TC 200-HTC: mechanical concrete properties at high temperatures—modelling and applications, Mater. Struct. 40 (2007) 841–853. doi:10.1617/s11527-007-9285-2.

[41] A. Fabien, M. Choinska, S. Bonnet, A. Pertué, A. Khelidj, Experimental study on the effect of aggregate size on the mechanical behavior and permeability of concrete,

Transf. 2012. (2012).

[42] NF EN 12390-13 AFNOR, Testing hardened concrete. Determination of secant modulus of elasticity in compression., (2013) 18–455.

[43] NF EN 12390-3 AFNOR, Testing hardened concrete. Compressive strength of test specimens., (2003).

[44] EUROCODE 2, Design of concrete structures – Part 1-2: General rules – structural fire design, TC 250. (2004).

[45] F. Bouziadi, B. Boulekbache, A. Haddi, C. Djelal, M. Hamrat, Numerical analysis of shrinkage of steel fiber reinforced high-strength concrete subjected to thermal loading, Constr. Build. Mater. 181 (2018) 381–393. doi:10.1016/J.CONBUILDMAT.2018.06.054.

[46] Y. Li, P. Pimienta, N. Pinoteau, K.H. Tan, Effect of aggregate size and inclusion of polypropylene and steel fibers on explosive spalling and pore pressure in ultra-high-performance concrete (UHPC) at elevated temperature, Cem. Concr. Compos. 99 (2019) 62–71. doi:10.1016/J.CEMCONCOMP.2019.02.016.

[47] V. Nguyen, Comportement des bétons ordinaire et à hautes performances soumis à haute température : application à des éprouvettes de grandes dimensions, Thèse de doctorat, Université de Cergy Pontoise, 2013.

[48] W. Khaliq, V. Kodur, Thermal and mechanical properties of fiber reinforced high performance self-consolidating concrete at elevated temperatures, Cem. Concr. Res. 41 (2011) 1112–1122. doi:10.1016/j.cemconres.2011.06.012.

[49] R. Jansson, Material properties related to fire spalling of concrete, Report, Lund Institute of technology, 2004.

[50] V. Kodur, Properties of Concrete at Elevated Temperatures, ISRN Civ. Eng. 2014 (2014) 1–15. doi:10.1155/2014/468510.

[51] P. Bamonte, P. Gambarova, Properties of Concrete Subjected to Extreme Thermal Conditions, J. Struct. Fire Eng. 5 (2014) 47–62.

[52] P. Pliya, A.-L. Beaucour, A. Noumowé., Contribution of cocktail of polypropylene and steel fibres in improving the behaviour of high strength concrete subjected to high temperature, Constr. Build. Mater. 25 (2011) 1926–1934.

doi:10.1016/j.conbuildmat.2010.11.064.

[53] E. Tolentino, F.S. Lameiras, .M. Gomes, V.W.L. Rigo da silva C.A., Effects of high temperature on residual performance of Portland cement concrete, Mater. Res. 5 (2002) 301–307.

[54] Z. Xing, A.-L. Beaucour, R. Hebert, A. Noumowe, B. Ledesert, Aggregate's influence on thermophysical concrete properties at elevated temperature, Constr. Build. Mater. 95 (2015) 18–28.

[55] R. Niry, A. Beaucour, R.L. Hebert, B. Ledesert, R. Bodet, A. Noumowe, High temperature behaviour of a wide petrographic range of siliceous and calcareous aggregates for concretes, Constr. Build. Mater. 123 (2016) 261–273. doi:10.1016/j.conbuildmat.2016.06.097.

[56] ACI, Code requirements for determining fire resistance of concrete and masonry construction assemblies., 216-1.07 Rep. by Jt. ACI/TMS Com. (2007) 32.

[57] EN 1994-1-2, Design of composite steel and concrete structures: General rules - structural fire design, EUROCODE 4 Part 1-2 Eur. Com. Stand. Brussels. (2004).

[58] M. Ezziane, L. Molez, T. Kadri, R. Jauberthie, F. Gouttefangeas, Adhérence fibre d'acier – matrice cimentaire dans les mortiers fibrés à hautes températures, Rencontres Univ. Assoc. Univ. Génie Civ. (2012) 1–10.

[59] V. V. Zhukov, Reasons of Explosive Spalling of Concrete by Fire, Bet. i Sjelezobet. 3 (1976) 26–28.

[60] R. Felicetti, F. Lo Monte, P. Pimienta, A new test method to study the influence of pore pressure on fracture behaviour of concrete during heating, Cem. Concr. Res. 94 (2017) 13–23. doi:10.1016/j.cemconres.2017.01.002.

[61] J.-C. Mindeguia, Contribution expérimentale à la compréhension des risques d'instabilité thermique des bétons, Thèse de doctorat, Université de Pau et des pays de l'Adour, 2009.

[62] R. Haniche, Contribution à l'étude des bétons portés en température / Evolution des propriétés de transfert / Etude de l'éclatement, Thèse de doctorat, Institut National des Sciences Appliquées de Lyon, 2011.